

Intravitreal Injection of AAV2 Transduces Macaque Inner Retina

Lu Yin,^{1,2} Kenneth Greenberg,^{3,4,5} Jennifer J. Hunter,^{1,2} Deniz Dalkara,³ Kathleen D. Kolstad,^{3,4,5} Benjamin D. Masella,⁶ Robert Wolfe,² Meike Visel,^{3,4,5} Daniel Stone,^{3,7} Richard T. Libby,^{1,2} David DiLoreto, Jr,¹ David Schaffer,^{3,7} John Flannery,^{3,4,5} David R. Williams,^{2,6} and William H. Merigan^{1,2}

PURPOSE. Adeno-associated virus serotype 2 (AAV2) has been shown to be effective in transducing inner retinal neurons after intravitreal injection in several species. However, results in nonprimates may not be predictive of transduction in the human inner retina, because of differences in eye size and the specialized morphology of the high-acuity human fovea. This was a study of inner retina transduction in the macaque, a primate with ocular characteristics most similar to that of humans.

METHODS. In vivo imaging and histology were used to examine GFP expression in the macaque inner retina after intravitreal injection of AAV vectors containing five distinct promoters.

RESULTS. AAV2 produced pronounced GFP expression in inner retinal cells of the fovea, no expression in the central retina beyond the fovea, and variable expression in the peripheral retina. AAV2 vector incorporating the neuronal promoter human connexin 36 (hCx36) transduced ganglion cells within a dense annulus around the fovea center, whereas AAV2 containing the ubiquitous promoter hybrid cytomegalovirus (CMV) enhancer/chicken- β -actin (CBA) transduced both Müller and ganglion cells in a dense circular disc centered on the fovea. With three shorter promoters—human synapsin (hSYN) and the shortened CBA and hCx36 promoters (smCBA and hCx36sh)—AAV2 produced visible transduction, as seen in fundus images, only when the retina was altered by ganglion cell loss or enzymatic vitreolysis.

From the ¹Flaum Eye Institute, the ²Center for Visual Science, ⁶Institute of Optics, University of Rochester, Rochester, New York; and the ³Helen Wills Neuroscience Institute and the Departments of ⁴Molecular and Cell Biology, ⁵Vision Science, and ⁷Chemical Engineering, University of California, Berkeley, Berkeley, California.

Supported by a grant from Bausch and Lomb, Inc.; National Institutes of Health (NIH) research Grants EY019375, BRP-EY014375, R01-HL081527, and NDC-5PN2EY018241; NIH Training Grant EY07125; NIH Core Grant EY001319; National Science Foundation (NSF) Science and Technology Center for Adaptive Optics (Santa Cruz, CA, managed by the University of California at Santa Cruz, cooperative agreement no. AST-9876783); and grants from the Foundation Fighting Blindness and Research to Prevent Blindness.

Submitted for publication July 20, 2010; revised October 18, 2010; accepted October 21, 2010.

Disclosure: L. Yin, None; K. Greenberg, None; J.J. Hunter, None; D. Dalkara, None; K.D. Kolstad, None; B.D. Masella, None; R. Wolfe, None; M. Visel, None; D. Stone, None; R.T. Libby, None; D. DiLoreto, Jr, None; D. Schaffer, None; J. Flannery, None; D.R. Williams, Bausch and Lomb (F, C, P, Optos (O); W.H. Merigan, Bausch and Lomb (F)

Corresponding author: William H. Merigan, Department of Ophthalmology and Center for Visual Sciences, Rochester, NY 14642; billm@cvs.rochester.edu.

CONCLUSIONS. The results in the macaque suggest that intravitreal injection of AAV2 would produce high levels of gene expression at the human fovea, important in retinal gene therapy, but not in the central retina beyond the fovea. (*Invest Ophthalmol Vis Sci*. 2011;52:2775–2783) DOI:10.1167/ios.10-6250

Virus-mediated gene delivery has been extensively studied for retinal transduction^{1,2} for basic research³ and clinical applications.^{4,5} Adeno-associated virus (AAV) is a preferred viral vector because of its lack of pathogenicity, high transduction efficiency, and long-term transgene expression,^{2,6,7} and it is typically administered by intravitreal injection to transduce inner retinal cells (e.g., ganglion and Müller cells). Of the many AAV serotypes that have been identified, serotype 2 is the most studied in the retina.^{8,9}

Although animal models of viral-mediated gene delivery to the retina are motivated by the development of human gene therapy, the uniqueness of the human eye may make viral transduction studies in common mammalian models (e.g., rats, mice, and rabbits) a poor predictor of transduction in humans. The macaque closely matches humans phylogenetically, as well as in structural features that may have an effect on retinal transduction, including eye size,^{10–12} the configuration of the high-acuity fovea,¹³ and a thick nerve fiber layer (NFL)¹⁴ and inner limiting membrane (ILM)¹⁵ on the retinal surface. However, only a handful of studies have explored AAV2 transduction in macaque eyes by intravitreal injection (Merigan WH, et al. *IOVS* 2008;49:ARVO E-Abstract 4514),^{6,16} and they suggest that the primate retina may have unique barriers to transduction that have not been identified in other animal models.

In this study, AAV2-mediated transduction of the macaque retina was performed by intravitreal injection, with green fluorescent protein (GFP) used as a reporter. Because of the biological significance of human foveal vision,^{17,18} one focus of our study was to evaluate the efficiency and selectivity of AAV2 with different promoters for transducing inner retinal cells in the fovea, which are excellent targets for retinal gene therapy. To this end, various neuronal (hCx36, hCx36sh, and hSYN) and ubiquitous (CBA and smCBA) promoters were evaluated. The GFP expression driven by those promoters was tracked over time with a fundus camera optimized to detect GFP fluorescence. When strong expression was reached, the subcellular localization of GFP expression was examined using fluorescence adaptive optics (AO) imaging,¹⁹ which provides substantially higher resolution and sensitivity than fundus imaging. These *in vivo* imaging results were then confirmed with histology. We found dense ganglion cell transduction with the hCx36 promoter in primate fovea, as well as nonselective transduction of Müller and ganglion cells with the ubiquitous CBA promoter. Moreover, our results showed that transduction

patterns of AAV2 in the macaque eye by intravitreal injection is qualitatively similar to that in the smaller eye of a foveated New World primate marmoset,^{20,21} yet significantly different from that in other species—in particular, rodent models.

METHODS

Subjects

Eight adult macaque monkeys were used, each weighing approximately 6 kg with ages ranging from 3 to 11 years at the time of injection (Supplementary Table S1, <http://www.iovs.org/lookup/suppl/doi:10.1167/iovs.10-6250/-DCSupplemental>). Eyes and retinas were normal in all the monkeys, except for one with a history of ganglion cell loss from a cortical infection and two that had been given intravitreal injections of microplasmin, which produces vitreoretinal detachment (Supplementary Materials and Methods, <http://www.iovs.org/lookup/suppl/doi:10.1167/iovs.10-6250/-DCSupplemental>). Head posts were implanted in the monkeys used for AO imaging, as previously described.¹⁹ All animal procedures were conducted according to the ARVO Statement for the Use of Animals in Ophthalmic and Vision Research and the guidelines of the Office of Laboratory Animal Care at the University of Rochester.

Viral Vectors

Preparation of Vectors. AAV vectors were packaged and purified by standard methods²² in the Flannery laboratory at the University of California, Berkeley. Briefly, AAV was packaged by triple transfection (Lipofectamine 2000; Invitrogen, Carlsbad, CA) of transfer and helper plasmids into AAV293 cells. After harvest, lysis, and iodixanol ultracentrifugation, the interphase between the 54% and 40% iodixanol fraction and the lower three quarters of the 40% iodixanol fraction were extracted and further purified by heparin-affinity chromatography. The eluent was concentrated and the buffer exchanged by using a centrifugal filter unit (Amicon Ultra-15; Millipore, Billerica, MA). The virus was washed three times with 15 mL of sterile phosphate-buffered saline (PBS) with 0.001% Tween. The vector was then titered by quantitative (q)PCR, relative to standards.

Promoter and Gene Payload of AAV2 Vector. The AAV vectors produced for this study were AAV2/2 (i.e., AAV2 inverted terminal repeat containing genomes packaged inside AAV2 capsid, termed AAV2 in this article), carrying the GFP (either the enhanced [e]GFP or humanized [h] GFP) transgene (Supplementary Table S1, <http://www.iovs.org/lookup/suppl/doi:10.1167/iovs.10-6250/-DCSupplemental>). One of the following five promoters (Table 1) was used to drive the transgenes: chicken-β-actin (CBA) with cytomegalovirus (CMV) enhancer, human connexin 36 (hCx36), human synapsin (hSYN), and shortened versions of CBA and hCx36 (smCBA and hCx36sh, respectively). In some cases, the transduction efficiency was evaluated by injection of 5 μL of the same vector into wild-type rat eyes. For primate injections, viral vectors were shipped on ice to the University of Rochester from the University of California (UC) Berkeley. The viral vector was then stored at 4°C until use, normally within 1 to 2 weeks. All in vivo imaging and histology were performed at the University of Rochester.

TABLE 1. Tested Promoters

Promoter	Symbol	Size (kb)	Reference
Chicken-β-actin promoter with cytomegalovirus enhancer	CBA	1.7	Boye SL, et al. <i>IOVS</i> 2006;47:ARVO E-Abstract 852 and Fitzsimons et al. ²³
Shortened CBA promoter	smCBA	0.95	Boye SL, et al. <i>IOVS</i> 2006;47:ARVO E-Abstract 852
Human connexin 36 promoter	hCx36	2.8	Greenberg K, PhD dissertation, UC Berkeley, 2007
Shortened hCx36 promoter	hCx36sh	1.8	Greenberg K, PhD dissertation, UC Berkeley, 2007
Human synapsin 1 gene promoter	hSYN	0.5	Kugler et al. ^{24,25}

The sequences of CBA and smCBA are described elsewhere (Boye SL, et al. *IOVS* 2006;47:ARVO E-Abstract 852).²³ The sequences of hCx36 and hCx36sh have not been published (Greenberg K, PhD dissertation, UC Berkeley, 2007). The 2.8-kb (hCx36) and 1.8-kb (hCx36sh) fragments of the hCx36 promoter were cloned from human genomic DNA by standard molecular biology techniques and high-fidelity PCR. The promoter fragments were then ligated into an AAV2 backbone vector containing GFP and the woodchuck post-transcriptional regulatory element (WPRE). All vectors were sequenced for PCR fidelity. The sequence of hSYN has been described by Kugler et al.^{24,25}

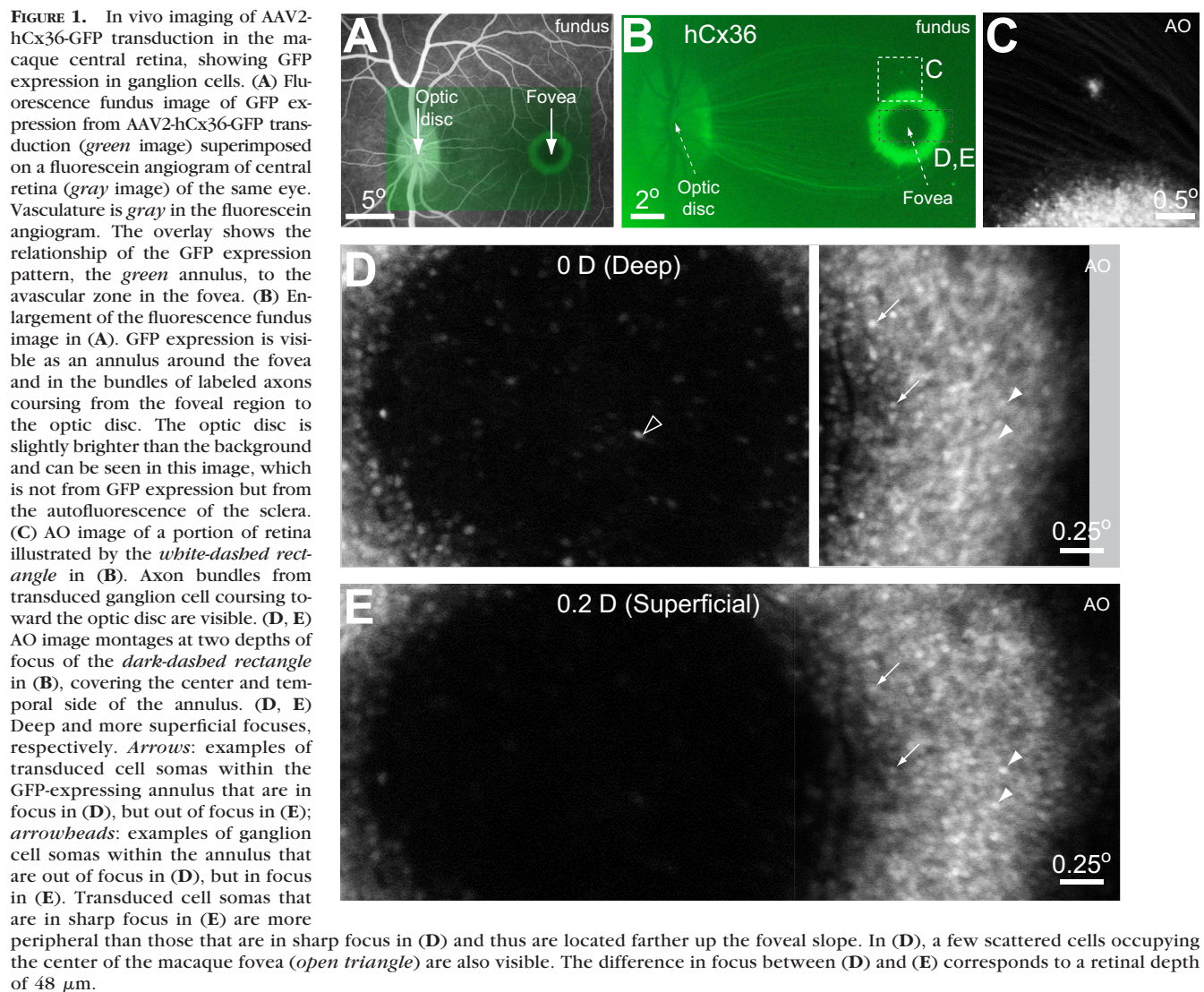
Intravitreal Injection. Viral vector (40–100 μL) was injected into the vitreous of each eye through the sclera approximately 3 mm behind the limbus, using a 30-gauge needle, with precautions taken to avoid infection. The condition of the injected eyes was monitored closely for up to 2 weeks. Three eyes from two animals were pretreated by an intravitreal injection of 50 μg (in 100 μL distilled water) of recombinant microplasmin (Thrombogenics, Leuven, Belgium; Supplementary Table S1, <http://www.iovs.org/lookup/suppl/doi:10.1167/iovs.10-6250/-DCSupplemental>), a recombinant serine protease that is used to degrade the vitreoretinal junction and produce posterior vitreal detachment in the human eye.²⁶ These injections were given in identical procedures 5 days before the injection of viral vector.

In cases in which both eyes were injected with vector, the second injection was performed less than 1 month after the first one (Supplementary Table S1, <http://www.iovs.org/lookup/suppl/doi:10.1167/iovs.10-6250/-DCSupplemental>), to avoid immune inactivation of the second injection by antibodies against AAV2 from the first injection.²⁷ Serum antibody titer against AAV2 was measured in the Schaffer laboratory at UC Berkeley (Supplementary Materials and Methods, <http://www.iovs.org/lookup/suppl/doi:10.1167/iovs.10-6250/-DCSupplemental>). We excluded from analysis one monkey that had a high serum antibody titer against AAV2 before vector injection (Supplementary Table S1, <http://www.iovs.org/lookup/suppl/doi:10.1167/iovs.10-6250/-DCSupplemental>).

In Vivo Transduction Evaluation

Fundus Imaging. Color and fluorescence fundus images were taken of each retina with a fundus camera (model TRC-50DX; Topcon, Paramus, NJ) that had been modified to image GFP fluorescence, by an excitation bandpass filter of 457 to 487 nm (FF01-472/30; Semrock, Rochester, NY) and a barrier filter with a bandpass of 502.5 to 537.5 nm (FF01-520/35; Semrock, Rochester, NY). Contrast and brightness of all fundus images presented in this article were adjusted (Photoshop; Adobe Systems, Waltham, MA) for better visualization of the relatively weak fluorescence signal of the GFP expressed in retinal neurons. Fundus images from the right eyes were flipped horizontally to match those from the left eyes, so that all fundus images presented herein have the same orientation. Scale bars for fundus images (Figs. 1A, 1B, 4A, 7) were calculated, assuming that the distance between the fovea center and temporal edge of the optic disc is 11.8°.²⁸

AO Imaging. A fluorescence adaptive optics scanning laser ophthalmoscope (FAOLSO) was used to image retinal neurons that expressed GFP in vivo, as described elsewhere.^{19,29} During imaging sessions, the monkeys were anesthetized with isoflurane at a dosage (typically 2%) sufficient to minimize large ocular movements and eliminate microsaccades. Images (1500 frames at a field of view of



2°–3°) were acquired simultaneously in two channels: (1) a reflectance channel that captured infrared light (794 ± 17 nm) reflected from cones and (2) a fluorescence channel that captured the fluorescence emission from GFP in retinal neurons excited by laser light at 488 nm.

To acquire through-focus images, we used a deformable mirror to focus the imaging plane through the depth of the retina. To equate diopters of focus (F) to axial distance (L , in micrometers) in the retina, we used the Elmsley model for an emmetropic eye¹⁹:

$$L = \frac{4}{3} \left[\frac{1}{D_{\text{eye}} + F} - \frac{1}{D_{\text{eye}}} \right] \times 10^6$$

where the D_{eye} is the power of the macaque eye. For the animals used in this study, a normative eye power of 74.2 D was assumed³⁰; 0.1 D corresponds to approximately 24 μ m.

Histology

Ex Vivo Preparation. For animals euthanized for histologic analysis (Supplementary Table S1, <http://www.iovs.org/lookup/suppl/doi:10.1167/iovs.10-6250/-DCSupplemental>), the eyes were enucleated from the animal immediately after euthanization and fixed by immersion in 4% paraformaldehyde (in 0.1 M phosphate buffer). The retina, with pigment epithelium attached, was separated from

the sclera. Retinal whole mounts were flattened on a glass slide by several radial cuts made at the periphery and covered with a coverslip with mounting medium (Vectashield; Vector Laboratories, Burlingame, CA). Transverse sections were prepared from retinal tissue embedded in agar and sectioned parallel to the horizontal raphe at 60- μ m thickness on a microtome with vibrating blade (Microm International GmbH, Walldorf, Germany).

Some samples were processed with immunostaining to increase the sensitivity of detection of GFP in the tissue. After they were washed in 0.01 M PBS and pretreatment solution (0.4% Triton X-100 in 0.01 M PBS), the retinas were incubated in blocking buffer (5% normal goat serum and 0.4% Triton X-100 in 0.01 M PBS) for 4 to 6 hours at room temperature followed by overnight at 4°C, to reduce nonspecific binding. We reacted the retinas with the primary antibody chicken anti-EGFP (Millipore Bioscience Research Reagents, Temecula, CA) at a dilution of 1:500. The reaction was performed initially at room temperature for 2 hours, then at 4°C for 3 to 4 days. After several washes in PBS, we reacted the retinas with the secondary antibody goat anti-chicken, conjugated with Alexa 488 (Invitrogen, Carlsbad, CA), to visualize the primary antibody staining (1–2 days, in dark at 4°C).

Ex Vivo Confocal Imaging. Ex vivo whole mount and transverse sections were imaged with a confocal microscope (LSM 510 Meta; Carl Zeiss Meditec, Thornwood, NY). GFP fluorescence in the

tissue or Alexa 488 signal after immunostaining were imaged with settings optimized for FITC. Image stacks were obtained across z -depths for whole mount tissue. The z -projection and transverse views of the image stacks were generated with NIH Image software (<http://rsb.info.nih.gov/nih-image/>). Brightness and contrast of the images presented in this article were adjusted (Photoshop; Adobe Systems, Waltham, MA) for better visualization. Montages of images from adjacent retinal regions were processed in the same program.

Conversion between Angular and Retinal Distances. Since *in vivo* fundus and AO images were measured in angular distance (degrees of visual angle) and *ex vivo* confocal imaging were measured in retinal distance (in micrometers), we assumed 223 μm in retinal distance for 1° in angular distance.³¹ Converted values are quoted in parentheses.

RESULTS

AAV2 transduction in the macaque eye occurred in the fovea and peripheral retina, but not in the central retina outside the fovea. Foveal transduction was more consistent across promoters than was peripheral transduction.

AAV2-hCx36-GFP Transduces Foveal Ganglion Cells, but Not Müller Cells

Intravitreal injection of AAV2-hCx36-GFP resulted in a dense annulus of GFP expression around the fovea, clearly visible *in vivo*, as evaluated with either fundus or AO imaging (Fig. 1; four eyes were tested; Supplementary Table S1, <http://www.iovs.org/lookup/suppl/doi:10.1167/iovs.10-6250/-DCSupplemental>). The inner edge of the annulus was approximately 1.5° (~0.3 mm) from the foveal center, which closely matches the location of the outer edge of the foveal avascular zone³² (Figs. 1A, 1B). The outer edge of the annulus was approximately 2.5° (~0.6 mm) from the fovea center. GFP-expressing axon bundles projecting from the annular ring formed an arcuate pattern converging on the temporal side of the optic disc (Fig. 1B).³³ Individual GFP-expressing cell bodies were visible in the AO images (Fig. 1C). The density of transduced cells declined gradually over approximately 100 μm , from GFP expression in many retinal cells at the outer edge of the annulus to expression below the detection limit (Figs. 1C, 2C, 2D). The first appearance of the transduction illustrated in these data was rapid, with the fluorescence signal of GFP first visible by fundus camera less than 1.5 months after injection into the eye shown in Figure 1A, and the expression remained stable for more than 2.5 years after vector injection.

Through-focus AO images of the GFP-expressing annulus showed a complete lack of GFP expression in the Müller cells with the neuronal hCx36 promoter (Figs. 1D, 1E). GFP-expressing cells in the inner portion of the annulus were in sharp view at deep focus (Fig. 1D, right, arrows), but not at the superficial focus (Fig. 1E, arrows), whereas GFP-expressing cells in the outer portion of the annulus were in sharp view at the superficial focus (Fig. 1E, arrowheads), but not at the deep focus (Fig. 1D, arrowheads). The deep-focus image (Fig. 1D) showed a few scattered cells within the foveal avascular zone (left, open triangle), which may be ganglion cells, as described by Grünert et al.³⁴

Ex vivo confocal images of retinal whole mounts confirmed AAV2-hCx36-GFP transduction in foveal cells in the ganglion cell layer (GCL), but did not involve Müller cells. Because ganglion cells comprise 95% of the neuronal cell population in the GCL in the fovea (displaced amacrine cells are 5% or less^{35,36}; see also Curcio and Allen¹³ for human retina), most of the GFP-expressing cells are ganglion cells. The inner edge of the GFP-expression annulus showed no expression of GFP in Müller cells below the ganglion cell layer (Fig. 2B), confirming

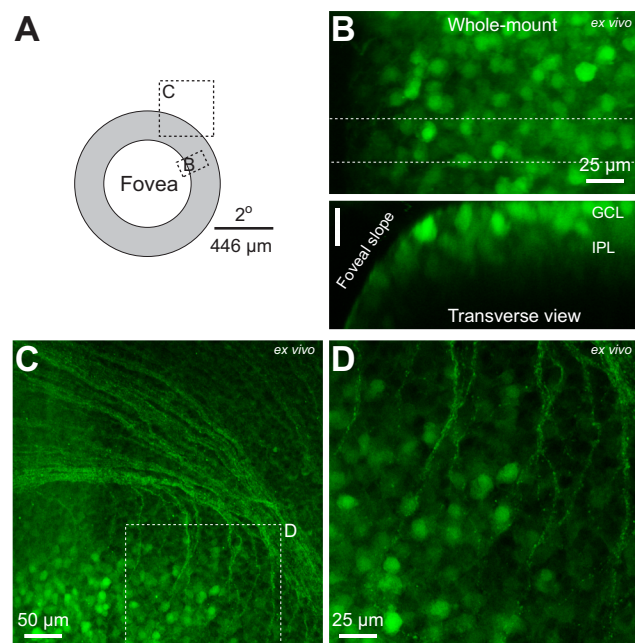


FIGURE 2. Ex vivo (histologic) evaluation of AAV2-hCx36-GFP transduction in the macaque central retina, showing dense GFP expression within the GCL in fovea. (A) Diagram of the foveal GFP expression, illustrating the location of the images in (B–D), which are from an eye transduced with AAV2-hCx36-GFP after treatment with microplasmin. Images in (B–D) show GFP expression within the ganglion cells and their axons, not amplified with immunostaining. (B) Confocal images of the inner edge of the annulus of GFP expression in whole mount view (top) and transverse view (bottom) reconstructed from the portion of the whole mount image stack between the two dashed horizontal lines. GFP expression is visible in GCL and IPL at retinal locations away from the foveal slope. NA, 1.2. (C) Confocal image of the outer edge of the annulus of GFP expression showing dense, expressing ganglion cells and their axons. NA, 0.8. (D) Higher magnification image that partially overlaps with the portion of (C) marked by the dashed rectangle. NA, 1.2.

the *in vivo* observation (Figs. 1D, 1E). The outer edge of the GFP-expression annulus also showed no intervening Müller cell processes between the individual cell somas in the GCL (Figs. 2C, 2D). GFP expression was also visible in the inner plexiform layer (IPL), where the dendrites of transduced ganglion cells extended (Fig. 2B). We also observed scattered GFP-expressing cell somas in the inner nuclear layer (INL), close to the IPL/INL border, which could have been amacrine cells³⁷ (data not shown).

While AAV2-hCx36-GFP produced strong foveal transduction in normal eyes, no retinal transduction of foveal GFP was seen in the central retinal outside the annulus (data not shown). In peripheral retina, we observed scattered transduction of cells in the GCL, especially along the blood vessels (data not shown). GFP expression was also found in the peripheral retina in eyes that received enzymatic vitreolysis with microplasmin before vector injection (see the Methods section and Supplementary Table S1, <http://www.iovs.org/lookup/suppl/doi:10.1167/iovs.10-6250/-DCSupplemental>). For the eye shown in Figure 3, GFP expression was visible in the Müller and retinal cells in both the GCL and INL at the distal edge of the far nasal peripheral retina, extending approximately 2 mm (~9°) toward the central retina. This peripheral transduction was visible in fundus images as dense GFP-expressing axons entering the optic disc from the nasal retina (data not shown).

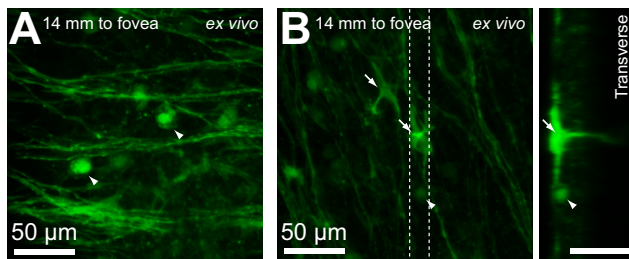


FIGURE 3. AAV2-hCx36-GFP transduction in the far peripheral retina after treatment with microplasmin. (**A, B**) GFP expression in ganglion cells (arrowheads) and Müller cells (arrows) from the nasal edge of the retina near the ora serrata. In the fluorescence fundus image of this eye, axon bundles from transduced ganglion cells were visible in the nerve fiber layer entering the optic disc from the nasal side (data not shown). In (**B**), the transverse view (right) was reconstructed from the portion of whole mount (*left*) image stack between the two *dashed vertical lines*. Transverse view shows the processes of the Müller cell (*arrow*) extending toward the outer retina. GFP expression was not amplified with immunostaining. NA, 1.2.

AAV2-CBA-GFP Transduced both Ganglion Cells and Müller Cells in the Fovea and the Peripheral Retina

Intravitreal injection of AAV2-CBA-GFP resulted in a disc of GFP expression centered on the fovea and extending to more than 1.5° (~ 0.3 mm) eccentricity, which was clearly visible *in vivo*, as evaluated by fundus and AO images (Figs. 4A–C; one eye was tested; Supplementary Table S1, <http://www.iovs.org/lookup/suppl/doi:10.1167/iovs.10-6250/-DCSupplemental>).

GFP expression in axon bundles appeared less intense with the CBA promoter than with the hCx36 promoter and could barely be seen in the fundus image (Fig. 4A compared with Fig. 1B). However, GFP-expressing axon bundles, as well as individual retinal cells, were clearly seen in AO images (Figs. 4B, 4C). GFP expression produced by AAV2-CBA-GFP took much longer to develop than AAV2-hCx36-GFP, with no funduscopically visible transduction, even at 4 months after viral injection, and the next examination at 10 months showed stable expression. However, the lower titer of the AAV2-CBA-GFP relative to the AAV2-hCx36-GFP precludes comparison of transduction efficiency of CBA and hCx36 promoters (Supplementary Table S1, <http://www.iovs.org/lookup/suppl/doi:10.1167/iovs.10-6250/-DCSupplemental>).

Through-focus AO images showed that foveal Müller cells are densely transduced. The three-dimensional morphology of the GFP-expressing Müller cells and distribution of ganglion cells in the foveal region were seen through a series of AO images across retinal depths from the outer retina toward the inner retina (Figs. 4D–G). In Figure 4D, Müller cell processes at the outer retina are in focus, while in Figure 4G, more superficial ganglion cell somas are in focus. The lateral displaced processes of the Müller cells and their somas were best visualized in the intermediate focuses (Figs. 4E, 4F, respectively). These GFP-expressing Müller cells were responsible for the solid, disclike appearance of the GFP expression in the fundus image (Fig. 4A).

Ex vivo confocal images confirmed that AAV2-CBA-GFP transduced both foveal ganglion cells and Müller cells (Fig. 5). As shown in the transverse section through the GFP-expressing

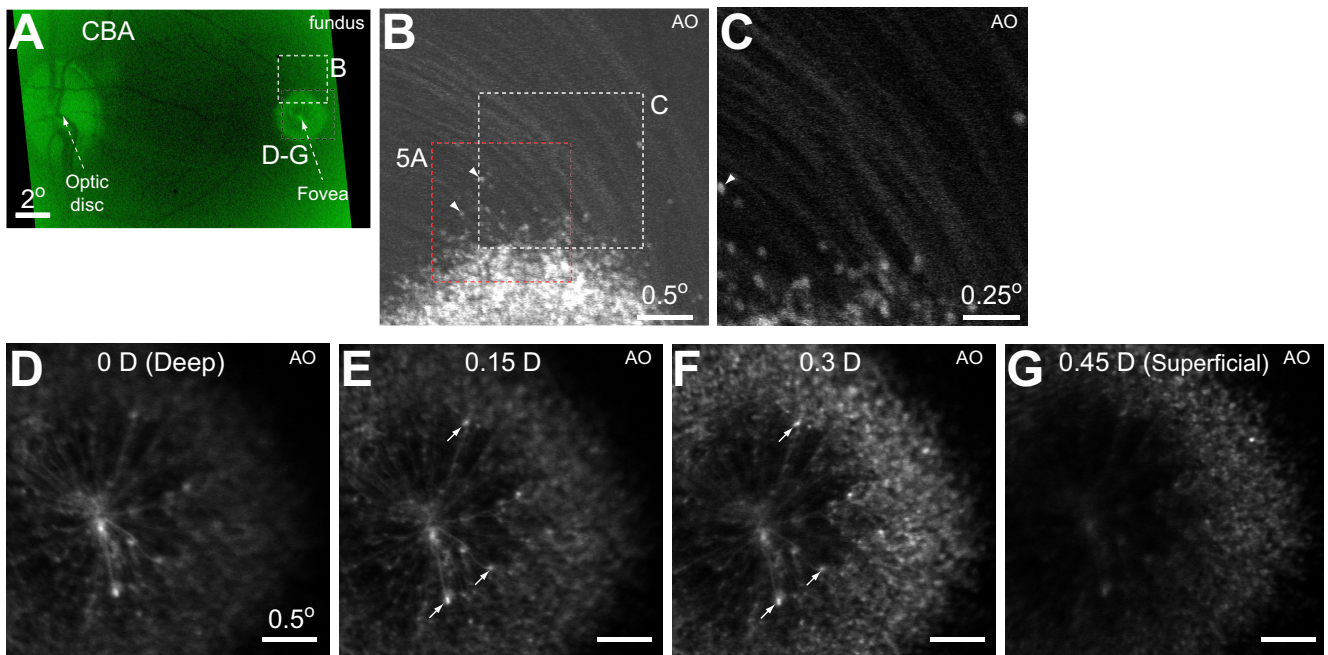


FIGURE 4. In vivo images of AAV2-CBA-GFP transduction in macaque central retina, showing GFP expression in both ganglion cells and Müller cells. (**A**) Fluorescence fundus image of GFP expression. A disc of GFP expression in Müller cells is centered on the fovea, with little GFP expression evident in the axon bundles originating from the fovea. (**B**) An AO image of a portion of retina illustrated by the *white-dashed rectangle* in (**A**). Axon bundles from transduced ganglion cells can be seen. The two cells labeled with *arrows* can be used as landmarks to visualize the relative alignment of (**C**) and Figure 5A. (**C**) Higher magnification AO image of the region marked in (**B**) with the *white-dashed rectangle*. At the edge of the disc of GFP expression, individual transduced retinal cells can be seen. *Arrowhead*: one of the two cells from (**B**). (**D–G**) Successive AO images of the center of the fovea (*the dark-dashed rectangle* in **A**) at four depths of focus, illustrating the variation in retinal structure. The deepest focus in (**D**) shows the most central processes of the Müller cells. The most superficial focus in (**G**) shows the foveal Müller cell processes out of focus and the more superficial ganglion cells in focus. (**E, F**) The intermediate focus steps, where the processes of Müller cells gradually extend from the outer retina toward the inner retina. A few Müller cell somas are labeled with *arrows* in (**E, F**). The focus step of 0.15 D corresponds to a retinal depth of 36 μ m. Scale bar: (**E–G**) same as in (**D**).

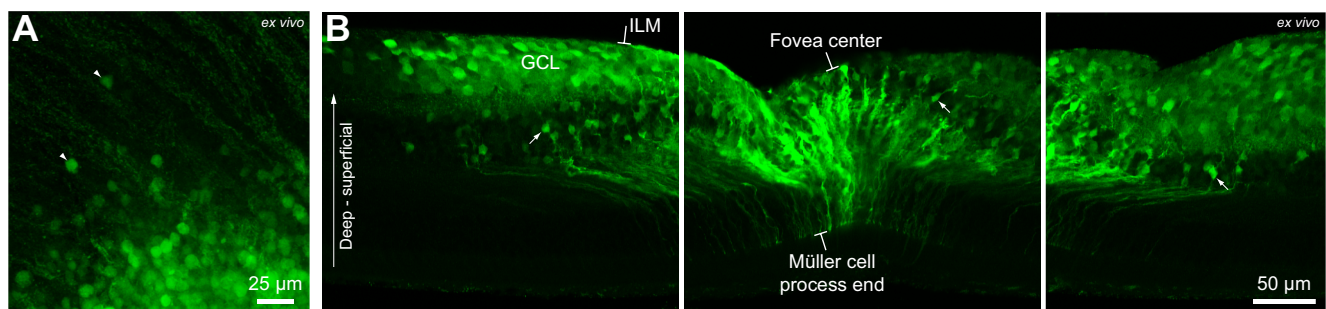


FIGURE 5. Ex vivo (histologic) evaluation of AAV2-CBA-GFP transduction in the macaque central retina. **(A)** Confocal image of the retinal region illustrated in Figure 4B by the red-dashed rectangle. The two retinal cells marked by arrowheads are the same cells marked by arrowheads in Figure 4B. **(B)** Confocal images of a transverse section through the center of the fovea, illustrating GFP expression in ganglion cell somas in the GCL surrounding the fovea and Müller cell processes extending from the outer to the inner retina. The images from left to right overlap, but differ slightly in focal plane. The sclerad end of the processes of GFP-expressing Müller cells were located close to the foveal center (deep), and gradually course away from the fovea center toward their vitread end in the ILM above the GCL. The thickness of the sections was 70 μ m. Arrows: Müller cell somas. **(A, B)** GFP expression was amplified with immunostaining; NA, 0.8.

disc centered on the fovea (Fig. 5B), GFP-expressing Müller cells extended their processes throughout the full thickness of the retina, with the sclerad end of their processes terminating near the outer limiting membrane (OLM) and the vitread end of their processes terminating at the ILM.³⁸ The lateral displacement between the sclerad and vitread ends of the Müller cell processes reflect the underlying anatomy: Müller cells ensheath cones in the fovea center that provide inputs to ganglion cells that are displaced away from the fovea center.³⁹ GFP-expressing ganglion cells extended to slightly greater eccentricity than did the Müller cells (Fig. 5B). Most GFP-expressing cell somas in the INL appeared to be Müller cells (Fig. 5B).

Transduction of peripheral retina by AAV2-CBA-GFP was evident in the ex vivo confocal images. The density of GFP-expressing retinal cells gradually increased from an eccentricity of approximately 8 mm ($\sim 30^\circ$) from the fovea center (data not shown) to the edge of the retina (Fig. 6A). Density of GFP-expressing retinal cells at the far peripheral retina was relatively sparse compared with that seen immediately around the fovea center (Fig. 6A compared with Fig. 5). As illustrated

by the example shown in Figures 6B–D from one far peripheral location, most of the GFP-expressing cells were Müller cells, and transduction in ganglion cells was less pronounced, such that the axons of these ganglion cells could not be seen in the fundus images (data not shown).

Shorter Promoters Were Ineffective in Normal Retinas, but Produced Transduction in Retinas with Ganglion Cell Loss, or Enzymatic Vitreolysis

Since AAV vectors have a limited packaging capacity, we explored the use of shorter neuronal and ubiquitous promoters to drive GFP expression in the primate retina.

We examined transduction by two short neuronal promoters—hSYN²⁴ and the shortened hCx36 promoter (hCx36sh)—in normal and diseased eyes with ganglion cell loss (one eye for each condition; Supplementary Table S1 and Supplementary Fig. S1, <http://www.iovs.org/lookup/suppl/doi:10.1167/iovs.10-6250/-DCSupplemental>) and compared both to transduction with the hCx36 promoter. As shown by the fundus images (Figs. 7A, 7C), intravitreal injection of AAV2 with neither promoter produced visible GFP expression in normal retinas over durations that exceeded the time needed for transduction by AAV2-hCx36, but in both cases (at comparable titer; Supplementary Table S1, <http://www.iovs.org/lookup/suppl/doi:10.1167/iovs.10-6250/-DCSupplemental>) produced visible GFP expression (Figs. 7B, 7D) in eyes with loss of ganglion cells (Supplementary Fig. S1A, <http://www.iovs.org/lookup/suppl/doi:10.1167/iovs.10-6250/-DCSupplemental>). However, the lower titers of the AAV2-hSYN-GFP and AAV2-hCx36sh-GFP than the AAV2-hCx36-GFP precluded comparison of the transduction efficiency of the two short neuronal promoters to hCx36 promoter (Supplementary Table S1, <http://www.iovs.org/lookup/suppl/doi:10.1167/iovs.10-6250/-DCSupplemental>).

We also examined the transduction by the short CBA promoter (smCBA) in a normal eye and in an eye that received enzymatic vitreolysis with microplasmin (see the Methods section; Supplementary Table S1, <http://www.iovs.org/lookup/suppl/doi:10.1167/iovs.10-6250/-DCSupplemental>) and compared both to the transduction with CBA promoter (at comparable titer; Supplementary Table S1, <http://www.iovs.org/lookup/suppl/doi:10.1167/iovs.10-6250/-DCSupplemental>). As shown by fundus images (Figs. 7E, 7F), intravitreal injection of AAV2-smCBA-GFP produced no visible GFP expression in normal retina (Fig. 7E) over a duration that exceeded the time needed to produce expression with the full-length CBA promoter, but produced visible GFP expression in the eye pretreated with mi-

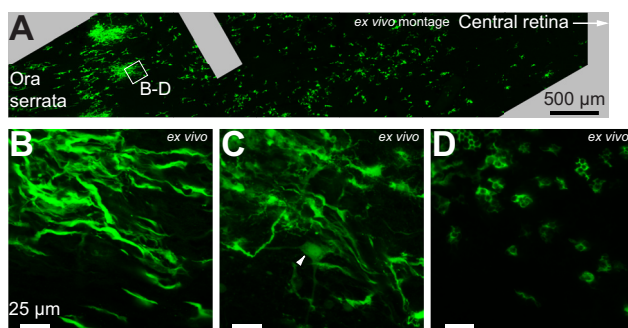


FIGURE 6. Ex vivo (histologic) images of AAV2-CBA-GFP transduced peripheral Müller and ganglion cells. **(A)** Montage of confocal images of a strip of peripheral retina extending from the ora serrata ~ 5.2 mm ($\sim 23^\circ$) toward the central retina, showing GFP expression in both scattered cells and clusters of cells. The density of transduced retinal cells declined toward the central retina (arrow). NA, 0.16. **(B–D)** Through-focus at higher magnification of the area marked by the rectangle in (A), showing GFP-expressing ganglion cells and Müller cells. Most transduced cells are Müller cells, shown as the dense GFP-expressing processes at the retinal surface (B) and the sclerad end of the processes (D; ~ 43 μ m deeper than B) in the outer retina. (C, arrow) A ganglion cell, ~ 11 μ m deeper than (B). In (A–D) GFP expression was amplified with immunostaining; NA, 1.2.

FIGURE 7. Fundus images illustrating three shorter promoters used with AAV2 that resulted in little or no visible GFP expression in normal retinas (**A, C, E**), but visible GFP expression in eyes with altered retinas (**B, D, F**). (**A, B**) Neuronal promoter, hSYN, produced no visible GFP expression after 4.5 months (**A**), but when injected into an eye with ganglion cell loss, (**B**) an annulus of GFP expression was seen in less than 2 months (data not shown; instead a later fundus image after 11 month is shown for better image quality). The transduction pattern in (**B**) is similar to that shown in Figure 1A, but the intensity of GFP expression is lower. (**C, D**) Shortened hCx36sh promoter resulted in no visible GFP expression after 4.5 months (**C**; for comparison, <2 months was typically needed for transduction by the full-length hCx36 promoter). However, when the promoter was injected into an eye with ganglion cell loss (**D**), a faint annulus of GFP expression around the fovea center was visible less than 3.5 months when the first fundus image was acquired (data not shown; instead a later fundus image after 4.5 months was shown for better image quality.) The transduction pattern in (**D**) was similar that shown in Figure 1A, but the intensity of GFP expression was lower. (**E, F**) Shortened CBA promoter (smCBA) resulted in no GFP expression after 15 months when injected into normal retina (**E**; for comparison, <10 months was needed for transduction by full-length CBA promoter). However, when injected into an eye that received enzymatic vitreolysis with microplasmin (**F**), GFP expression in fovea was visible in less than 4.5 months, when the first fundus image was acquired (data not shown; instead a later fundus image after 10 months is shown for better image quality). The transduction pattern in (**F**) was similar to that shown in Figure 4A.

croplasmin (Fig. 7F). For the latter, the appearance of foveal transduction (Fig. 7F) was similar to that of the full-length CBA promoter (Fig. 4A), and we confirmed by histology that both foveal ganglion cells and Müller cells were transduced (data not shown). Besides foveal transduction, prominent transduction in far peripheral ganglion cells was visible in the fundus image (Fig. 7F) as dense GFP expression in axons entering the optic disc from the nasal retina, and we verified by histology that both Müller cells and ganglion cells at the distal edge of far peripheral retina were transduced (data not shown).

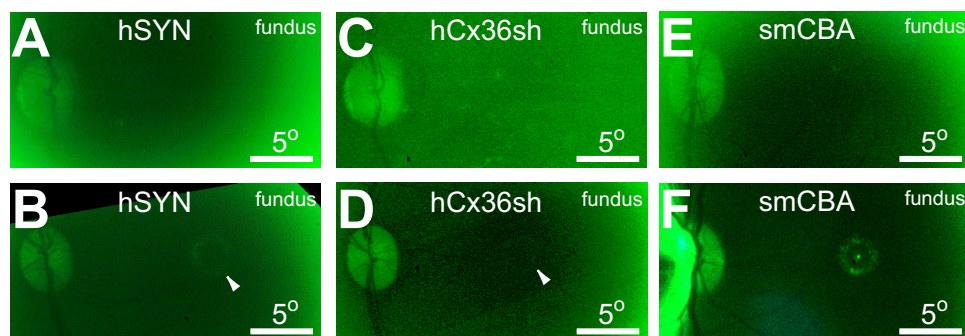
DISCUSSION

In this study, intravitreal injection of AAV2 into the macaque eye produced dense ganglion cell and Müller cell transduction in only a narrow region surrounding the fovea, with no transduction in the central retina beyond the fovea and little or no transduction in the peripheral retina. This result differs from the more uniform transduction reported after intravitreal injection in other species, including rodents,^{8,40} and raises the question of how well studies in nonprimates are predictive of gene therapy results in humans.

What Limits Transduction of the Macaque Inner Retina?

The limited transduction we observed may have been due to the physical barriers posed by the anatomy of the macaque retina, such as the NFL and ILM, which lie along the surface of the retina, between the GCL and vitreous.

The variation in thickness of the NFL across the retina is consistent with the transduction patterns observed in this study. There is little NFL covering the foveal retinal location where inner retinal cells were transduced (Figs. 1B, 4A). Outside the fovea, superior and inferior to the optic disc, NFL thickness can reach a maximum thickness of more than 200 μm in the macaque retina and more than 300 μm in the human retina.¹⁴ These are the regions where no transduction was observed. When NFL thickness was greatly reduced in retinas with ganglion cell loss, inner retina transduction was enhanced (Figs. 7B, 7D; Supplementary Fig. S1, <http://www iovs org/lookup/suppl/doi:10.1167/iosv.10-6250/-DCSupplemental>). A similar phenomenon has been reported in degenerated rodent retina.⁴¹ Together, these results suggest enhanced transduction in the



disease-compromised retina, an advantage from the gene-delivery perspective.

Although the ILM is thin compared with the NFL, its thickness is inversely related to the inner retinal transduction efficiency observed in this study. Macaque (and human) ILM is thinnest in the fovea, where transduction was best, moderately thicker in the far peripheral retina, where expression was modest, and thickest in the posterior retina near the fovea, where almost no transduction was observed.¹⁵ Furthermore, the ILM is thinner above the retinal vessels,¹⁵ where we observed focal transduction of retinal cells along blood vessels at eccentricities beyond approximately 30° (data not shown). Microplasmin, which disrupts the border between the vitreous and ILM, increased transduction by AAV2-hCx36 and AAV2-smCBA in the far peripheral retina where the ILM is relatively thin, similar to the increased transduction in rodent when the ILM was disrupted by a protease.⁴² The human and macaque ILM are very similar,¹⁵ and thus the ILM is a likely a barrier to AAV-mediated gene delivery in humans.

The pattern of foveal transduction could also reflect other features of the primate retina that interact with AAV2 capsids, such as the distribution of cell surface receptors, since AAV2 binds selectively to heparin sulfate proteoglycan and three co-receptors.^{43–47} The topographic distribution of these receptors has not been measured in macaque retina. However, the dense transduction at the fovea indicates that promoter selectivity is not the basis for a lack of transduction in other areas of retina.

Which Animal Models Are Optimal for Developing Human Gene Therapy?

The wide variety of animal models used in gene therapy research each fills an important role. Rodents (e.g., mice) are widely used species that are well-suited for genetic manipulations, whereas dogs and cats provide several unique models of retinal degeneration and greater similarity to human retina because of the large eye size and higher acuity area centralis. The nonhuman primate is better suited than the other species for predicting transduction in humans because of the unique morphology of the retina in species that have a fovea.

Recently, transduction of the inner retina by intravitreal injection was studied in one nonhuman primate, the New World marmoset,²⁰ using an AAV2 virus with either the CAG

(hybrid CMV early enhancer/chicken β -actin) or CMV (human cytomegalovirus immediate early gene) promoter.²¹ The marmoset has a small eye, with an average axial length of 11 mm,⁴⁸ substantially smaller than that of the macaque (18 mm)⁴⁹ and human (24 mm).⁵⁰ Marmosets have a well-developed fovea, similar to that of the macaque and humans⁵¹ in both overall shape and the extent of ganglion cell displacement away from the foveal center.

However, the transduction of marmoset retina observed by Ivanova et al.²¹ was quite different from that observed in the macaque in our laboratory in three respects: cellular selectivity, the spatial pattern of transduction across the retina, and the depth of transduction through the retina. The CBA promoter used in the present study and the CAG promoter used in the marmoset study of Ivanova et al.²¹ are similar.²³ Despite this similarity, the macaque showed Müller cell and ganglion cell transduction at the fovea and largely Müller cell transduction in peripheral retina, while the marmoset showed no Müller cell transduction at any retinal location, but substantial ganglion cell transduction across the retina. The spatial pattern of transduction across the retina was also different, with the macaque showing dense GFP expression in foveal ganglion cells, but little GFP expression in peripheral ganglion cells, while the marmoset showed relatively sparse foveal ganglion cell transduction, but substantial peripheral ganglion cell transduction. Finally, the depth of transduction through the retina also differed between the macaque and marmoset. Neuronal transduction in the macaque retina was confined to the GCL and inner portion of the INL, whereas the transduction in the marmoset extends to outer retina (e.g., photoreceptors).

We speculate that these differences between the macaque and marmoset could be due both to species differences in viral tropism and to a difference in the topology of a physical barrier, such as the ILM, which has not been studied in the marmoset. Given that the macaque is closer to humans in evolutionary lineage⁵² and that there is great similarity in physical attributes of the two species, such as eye size⁵³ and ILM thickness,¹⁵ it is likely that the transduction observed in macaques in this study provides a closer prediction of transduction by intravitreal injection in humans than that observed in the marmoset. However, further research is needed, due to differences in promoter, age, and viral titer between the studies in the two species.

Choice of Vector and Promoter for Transducing Macaque Inner Retina

AAV2, with the hCx36 promoter, produced selective transduction of foveal ganglion cells, but not of Müller cells, making it a good choice for inserting gene products into ganglion cells for neurophysiology studies or ganglion cell neuroprotection in diseases such as glaucoma. However, the hCx36 promoter fragment used in this study was large (2.8 kb), and it occupies much of the 4.7-kb genomic capacity of AAV2,⁵⁴ leaving little space for transgenes substantially larger than GFP (0.7 kb). The CBA promoter (1.7 kb) is smaller than hCx36 and produces good transduction of both foveal and peripheral ganglion cells and Müller cells. The major drawback of the CBA promoter was the extended time until expression occurred.

The short promoters—hSYN, hCx36sh, and smCBA—did not produce visible transduction in healthy retina over an extended time and thus are not effective choices for use in macaques. Although the smCBA promoter yielded similar expression to full-length CBA when injected into an eye pre-treated with microplasmin, the hCx36sh and hSYN promoters remained ineffective, even when injected into eyes altered by ganglion cell loss. That the AAV2 vectors with two of these

promoters (smCBA and hSYN) have produced excellent retinal transduction in other mammals (Boye SL, et al. *IOVS* 2006;47: ARVO E-Abstract 852)^{7,42,55} illustrates the unique difficulty in achieving gene expression in the primate retina.

The Importance of In Vivo, High-Resolution AO Imaging in Monitoring Viral Transduction in the Macaque

Although histologic verification remains the standard method for evaluating the efficiency and selectivity of transduction by viral vectors, *in vivo* imaging is particularly important in investigating therapeutic effects of gene therapy in primates, as it can eliminate the need to serially kill different animals for histology. Fundus imaging can reveal the time course and spatial pattern of expression in each animal. Because AO imaging has substantially greater sensitivity and spatial resolution than fundus imaging, as well as axial sectioning capacity (through-focus; Figs. 1D, 1E, 4D-G), it is able to reveal details of GFP expression that could not be determined from the fundus images. This distinction was particularly evident in this study when visualizing ganglion cell transduction by CBA, which was clear in the AO images (Figs. 4B-G), but barely observable in the fundus image (Fig. 4A).

Implications of This Study for Human Retinal Gene Therapy

A significant issue in moving viral-mediated gene therapies for human retinal disease from small animal efficacy studies to clinical applications is the potential differences between the eye and retina of the animal model and the human (e.g., retinal cell-surface properties, promoter selectivity, and anatomy of the retina). Studies in the ideal animal model, the macaque monkey, are severely limited by availability, cost, and lack of appropriate disease models, but must be performed to develop successful retinal gene therapy for humans. This study demonstrates that barriers to transduction of the inner retina in the macaque are substantial, but also shows that the use of high-resolution, *in vivo* adaptive optics imaging greatly facilitates such investigations.

Acknowledgments

The authors thank Jennifer Strazzeri (Flaum Eye Institute, University of Rochester) for technical assistance, surgery, and fundus photography and Thurma McDaniel and Tracey Bubel (Center for Visual Science, University of Rochester) for assistance with histology.

References

- Harvey AR, Hu Y, Leaver SG, et al. Gene therapy and transplantation in CNS repair: the visual system. *Prog Retin Eye Res.* 2006; 25:449–489.
- Daya S, Berns KI. Gene therapy using adeno-associated virus vectors. *Clin Microbiol Rev.* 2008;21:583–593.
- Mancuso K, Hauswirth WW, Li Q, et al. Gene therapy for red-green colour blindness in adult primates. *Nature.* 2009;461:784–787.
- Tan MH, Smith AJ, Pawlyk B, et al. Gene therapy for retinitis pigmentosa and Leber congenital amaurosis caused by defects in AIPL1: effective rescue of mouse models of partial and complete Aip1 deficiency using AAV2/2 and AAV2/8 vectors. *Hum Mol Genet.* 2009;18:2099–2114.
- Maguire AM, High KA, Auricchio A, et al. Age-dependent effects of RPE65 gene therapy for Leber's congenital amaurosis: a phase 1 dose-escalation trial. *Lancet.* 2009;374:1597–1605.
- Lebherz C, Auricchio A, Maguire AM, et al. Long-term inducible gene expression in the eye via adeno-associated virus gene transfer in nonhuman primates. *Hum Gene Ther.* 2005;16:178–186.

7. Petrus-Silva H, Dinculescu A, Li Q, et al. High-efficiency transduction of the mouse retina by tyrosine-mutant AAV serotype vectors. *Mol Ther.* 2009;17:463–471.
8. Hellstrom M, Ruitenberg MJ, Pollett MA, et al. Cellular tropism and transduction properties of seven adeno-associated viral vector serotypes in adult retina after intravitreal injection. *Gene Ther.* 2009;16:521–532.
9. Surace EM, Auricchio A. Versatility of AAV vectors for retinal gene transfer. *Vision Res.* 2008;48:353–359.
10. Rolling F. Recombinant AAV-mediated gene transfer to the retina: gene therapy perspectives. *Gene Ther.* 2004;11(suppl 1):S26–S32.
11. Buch PK, Bainbridge JW, Ali RR. AAV-mediated gene therapy for retinal disorders: from mouse to man. *Gene Ther.* 2008;15:849–857.
12. Stieger K, Lheriteau E, Moullier P, Rolling F. AAV-mediated gene therapy for retinal disorders in large animal models. *ILAR J.* 2009;50:206–224.
13. Curcio CA, Allen KA. Topography of ganglion cells in human retina. *J Comp Neurol.* 1990;300:5–25.
14. Frenkel S, Morgan JE, Blumenthal EZ. Histological measurement of retinal nerve fibre layer thickness. *Eye (Lond).* 2005;19:491–498.
15. Matsumoto B, Blanks JC, Ryan SJ. Topographic variations in the rabbit and primate internal limiting membrane. *Invest Ophthalmol Vis Sci.* 1984;25:71–82.
16. Lebherz C, Maguire AM, Auricchio A, et al. Nonhuman primate models for diabetic ocular neovascularization using AAV2-mediated overexpression of vascular endothelial growth factor. *Diabetes.* 2005;54:1141–1149.
17. Cheung SH, Legge GE. Functional and cortical adaptations to central vision loss. *Vis Neurosci.* 2005;22:187–201.
18. Harrison ER. Visual acuity and the cone cell distribution of the retina. *Br J Ophthalmol.* 1953;37:538–542.
19. Gray DC, Wolfe R, Gee BP, et al. In vivo imaging of the fine structure of rhodamine-labeled macaque retinal ganglion cells. *Invest Ophthalmol Vis Sci.* 2008;49:467–473.
20. Troilo D, Howland HC, Judge SJ. Visual optics and retinal cone topography in the common marmoset (*Callithrix jacchus*). *Vision Res.* 1993;33:1301–1310.
21. Ivanova E, Hwang GS, Pan ZH, Troilo D. Evaluation of AAV-mediated expression of Chop2-GFP in the marmoset retina. *Invest Ophthalmol Vis Sci.* 2010;51:5288–5296.
22. Zolotukhin S, Byrne BJ, Mason E, et al. Recombinant adeno-associated virus purification using novel methods improves infectious titer and yield. *Gene Ther.* 1999;6:973–985.
23. Fitzsimons HL, Bland RJ, During MJ. Promoters and regulatory elements that improve adeno-associated virus transgene expression in the brain. *Methods.* 2002;28:227–236.
24. Kugler S, Lingor P, Scholl U, Zolotukhin S, Bahr M. Differential transgene expression in brain cells in vivo and in vitro from AAV-2 vectors with small transcriptional control units. *Virology.* 2003;311:89–95.
25. Kugler S, Kilic E, Bahr M. Human synapsin 1 gene promoter confers highly neuron-specific long-term transgene expression from an adenoviral vector in the adult rat brain depending on the transduced area. *Gene Ther.* 2003;10:337–347.
26. Gandorfer A, Rohleder M, Sethi C, et al. Posterior vitreous detachment induced by microplasmin. *Invest Ophthalmol Vis Sci.* 2004;45:641–647.
27. Li Q, Miller R, Han PY, et al. Intraocular route of AAV2 vector administration defines humoral immune response and therapeutic potential. *Mol Vis.* 2008;14:1760–1769.
28. Kolb H, Fernandez E, Nelson R. Facts and figures concerning the human retina. In: Kolb H, Fernandez E, Nelson R, eds. *Webvision: The Organization of the Retina and Visual System.* Salt Lake City: University of Utah, John Moran Eye Center; 2007.
29. Gray DC, Merigan W, Wolfing JI, et al. In vivo fluorescence imaging of primate retinal ganglion cells and retinal pigment epithelial cells. *Opt Express.* 2006;14:7144–7158.
30. Lapuerta P, Schein SJ. A four-surface schematic eye of macaque monkey obtained by an optical method. *Vision Res.* 1995;35:2245–2254.
31. Perry VH, Cowey A. The ganglion cell and cone distributions in the monkey's retina: implications for central magnification factors. *Vision Res.* 1985;25:1795–1810.
32. Snodderly DM, Weinhaus RS, Choi JC. Neural-vascular relationships in central retina of macaque monkeys (*Macaca fascicularis*). *J Neurosci.* 1992;12:1169–1193.
33. Ogden TE. Nerve fiber layer of the macaque retina: retinotopic organization. *Invest Ophthalmol Vis Sci.* 1983;24:85–98.
34. Grünert U, Greferath U, Boycott BB, Wassle H. Parasol (P alpha) ganglion-cells of the primate fovea: immunocytochemical staining with antibodies against GABA_A-receptors. *Vision Res.* 1993;33:1–14.
35. Wassle H, Grünert U, Rohrenbeck J, Boycott BB. Cortical magnification factor and the ganglion cell density of the primate retina. *Nature.* 1989;341:643–646.
36. Wassle H, Grünert U, Rohrenbeck J, Boycott BB. Retinal ganglion cell density and cortical magnification factor in the primate. *Vision Res.* 1990;30:1897–1911.
37. Ahmad KM, Klug K, Herr S, Sterling P, Schein S. Cell density ratios in a foveal patch in macaque retina. *Vis Neurosci.* 2003;20:189–209.
38. Distler C, Dreher Z. Glia cells of the monkey retina: II, Müller cells. *Vision Res.* 1996;36:2381–2394.
39. Schein SJ. Anatomy of macaque fovea and spatial densities of neurons in foveal representation. *J Comp Neurol.* 1988;269:479–505.
40. Ali RR, Reichel MB, De Alwis M, et al. Adeno-associated virus gene transfer to mouse retina. *Hum Gene Ther.* 1998;9:81–86.
41. Kolstad KD, Dalkara D, Guerin K, et al. Changes in adeno-associated virus-mediated gene delivery in retinal degeneration. *Hum Gene Ther.* 2010;21:571–578.
42. Dalkara D, Kolstad KD, Caporale N, et al. Inner limiting membrane barriers to AAV-mediated retinal transduction from the vitreous. *Mol Ther.* 2009;17:2096–2102.
43. Summerford C, Samulski RJ. Membrane-associated heparan sulfate proteoglycan is a receptor for adeno-associated virus type 2 viruses. *J Virol.* 1998;72:1438–1445.
44. Summerford C, Bartlett JS, Samulski RJ. AlphaVbeta5 integrin: a co-receptor for adeno-associated virus type 2 infection. *Nat Med.* 1999;5:78–82.
45. Bartlett JS, Wilcher R, Samulski RJ. Infectious entry pathway of adeno-associated virus and adeno-associated virus vectors. *J Virol.* 2000;74:2777–2785.
46. Bartlett JS, Samulski RJ, McCown TJ. Selective and rapid uptake of adeno-associated virus type 2 in brain. *Hum Gene Ther.* 1998;9:1181–1186.
47. Qing K, Mah C, Hansen J, Zhou S, Dwarki V, Srivastava A. Human fibroblast growth factor receptor 1 is a co-receptor for infection by adeno-associated virus 2. *Nat Med.* 1999;5:71–77.
48. Troilo D, Nickla DL. The response to visual form deprivation differs with age in marmosets. *Invest Ophthalmol Vis Sci.* 2005;46:1873–1881.
49. Qiao-Grider Y, Hung LF, Kee CS, Ramamirtham R, Smith EL, 3rd. Recovery from form-deprivation myopia in rhesus monkeys. *Invest Ophthalmol Vis Sci.* 2004;45:3361–3372.
50. Kubo E, Kumamoto Y, Tsuzuki S, Akagi Y. Axial length, myopia, and the severity of lens opacity at the time of cataract surgery. *Arch Ophthalmol.* 2006;124:1586–1590.
51. Hendrickson AE. Organization of the adult primate fovea. In: Penfold PL, Provis JM, eds. *Macular Degeneration.* Berlin: Springer; 2005:1–23.
52. Lewin R. *Human Evolution: an Illustrated Introduction.* 5th ed. Oxford, UK: Blackwell Publishing Ltd; 2005.
53. Qiao-Grider Y, Hung LF, Kee CS, Ramamirtham R, Smith EL, 3rd. Normal ocular development in young rhesus monkeys (*Macaca mulatta*). *Vision Res.* 2007;47:1424–1444.
54. Dong JY, Fan PD, Frizzell RA. Quantitative analysis of the packaging capacity of recombinant adeno-associated virus. *Hum Gene Ther.* 1996;7:2101–2112.
55. Geng Y, Greenberg KP, Wolfe R, et al. In vivo imaging of microscopic structures in the rat retina. *Invest Ophthalmol Vis Sci.* 2009;50:5872–5879.